Journal of Alloys and Compounds 509 (2011) 1619–1625

Contents lists available at ScienceDirect

Journal of Alloys and Compounds

journal homepage: www.elsevier.com/locate/jallcom

3R and 14M martensitic transformations in as-rolled and annealed $Ni_{64}Al_{34.5}Re_{1.5}$ shape memory alloy

Hui-Jang Kang, Shyi-Kaan Wu*, Ling-Mei Wu

Department of Materials Science and Engineering, National Taiwan University, Taipei 106, Taiwan

ARTICLE INFO

Article history:
Received 16 September 2010
Received in revised form 3 November 2010
Accepted 5 November 2010
Available online 18 November 2010

Keywords:
NiAlRe alloy
Shape memory
Martensitic transformation
Microstructure
X-ray diffraction
Transmission electron microscopy, TEM

ABSTRACT

Martensitic transformation of as-rolled and 1323 K × 1 h annealed $Ni_{64}Al_{34.5}Re_{1.5}$ (NiAl–1.5Re) shape memory alloy (SMA) is investigated. For as-rolled NiAl–1.5Re alloy, TEM and EPMA results indicate both 14M and 3R martensites are observed at the room temperature. 14M is formed in the precipitate-free zone which is a Ni-depletion region and 3R is formed in the matrix which is a Ni-enrichment region. XRD and partial-cycle DSC testing results show that the higher temperature peak of the DSC cooling curve is B2 → 14M and the lower one is B2 → 3R. Hardness tests show that 14M hardness is higher than that of 3R. For annealed NiAl–1.5Re alloy, only B2 ↔ 3R can be observed. The critical value for the formation of 14M martensite in NiAl–1.5Re alloy is about 63.6 at.% Ni, as compared to 63.0 at.% Ni for Ni–Al binary SMAs.

1. Introduction

The Ni-rich Ni–Al binary alloys with 62–69 at.% Ni are well-known shape memory alloys (SMAs) with high martensitic transformation starting temperatures (M_s), high thermal conductivity, high temperature strength and excellent oxidation/corrosion resistance [1,2]. Previous studies indicate that Ni-rich Ni–Al SMAs exhibit B2 ↔ 3R martensitic transformation with 3R martensite having a multiply twinned tetragonal $L1_0$(3R) structure. However, another 14M martensite (formerly named as 7R or 7M martensite [3]) has also been observed when the Ni content is lower than 63 at.% [4,5]. The M_s temperature of Ni–Al binary SMAs is very sensitive to the alloy composition in which a change in nickel content by as little as 1 at.% would vary the alloy's M_s temperature by about 200 K [1,6].

For Ni–Al binary SMAs with Al content ≥37 at.% and $M_s \leq 273$ K, the stress-induced 14M martensite can be observed at room temperature [7,8]. Meanwhile, in some Ni–Al ternary SMAs, such as Ni–Al–Fe alloys aged at 673 K for long time, the 14M martensite appears as fine precipitates in the matrix [9]. In the Ni–Al–Mn ternary SMAs with Mn content ≥30%, the appearance of 14M martensite has also been observed [10]. The structure of the 14M martensite of $Ni_{63.1}Al_{36.9}$ binary SMA was firstly studied by Martynov et al. [5] and was regarded as a long period structure of $L1_0$ with a complex arrangement of periodic stacking faults induced by external tension at room temperature. In 1990, Schryvers et al. observed the tweed structure prior to the martensitic transformation in $Ni_{62.5}Al_{37.5}$ binary SMA by high resolution transmission electron microscope (TEM) and considered the (micro)tweed as a precursor to the 14M stacking [8]. In 1991, Khachaturyan et al. [11] introduced the 14M martensite as an adaptive phase in which the adaptive martensite is formed as an elastically constrained phase when the scale of the structure heterogeneities induced by the crystal-strain accommodation is reduced to the microscopic scale of the twin-plane interplanar distance. In 1993, Khadkikar et al. [12] studied the $Ni_{63}Al_{37}$ binary alloy fabricated by powder metallurgy (PM). From TEM observation, they indicated that both 3R and 14M martensites are transformed in the short-time aged specimens due to the formation of Ni_2Al leading to Ni-enriched and Ni-depleted areas, respectively. Meanwhile, Murthy and Goo [13] studied on the as-quenched $Ni_{63.1}Al_{36.9}$ binary alloy and found it was total 3R martensite at room temperature. After this alloy was aged at 723 K for 6 h, Ni_2Al precipitates were observed in the matrix and 14M martensite appeared as well. They suggested that the 14M martensite is an "adaptive" phase [11] and can be regarded as 3R martensite microtwinned on its $\{1\,1\,1\}_{3R}$ planes to provide an invariant strain. In 1994, George et al. [14] discovered that the as-quenched $Ni_{64}Al_{36}$ binary alloy was 3R martensite at room temperature and it transformed to B2 + ω-like phase by heating the alloy up to 873 K. After cooling the alloy back to room

* Corresponding author at: Department of Materials Science and Engineering, National Taiwan University, 1, Roosevelt Rd., Sec. 4, Taipei 106, Taiwan.
Tel.: +886 2 2363 7846; fax: +886 2 2363 4562.
E-mail address: skw@ntu.edu.tw (S.-K. Wu).

0925-8388/$ – see front matter © 2010 Elsevier B.V. All rights reserved.
doi:10.1016/j.jallcom.2010.11.052

temperature, it showed Ni_5Al_3 phase and 3R + 14M martensites. Also in 1994, Yang and Wayman [9] found 14M martensite exhibited in $Ni_{60}Al_{25}Fe_{15}$ ternary alloy. They observed a progressive microstructural evolution from 3R to 14M martensite with aging in the B2 phase due to the Ni-depletion effect in the matrix caused by the Ni-enrichment in the G.P. zone. As Yang and Wayman proposed, in 1997, Potapov et al. [15] studied the PM-fabricated $Ni_{64}Al_{36}$ and $Ni_{65}Al_{35}$ alloys by X-ray diffraction (XRD) and suggested that a progressive transition of the martensitic structure from 3R to 14M due to the concentration inhomogeneities induced by the nucleation of Ni_2Al phase. In 2000, Potapov et al. [16] also reported that the nanoscale inhomogeneities in melt-spun Ni–Al alloy can appear B2 → 3R or 14M martensitic transformation. Their study suggested that for as-spun $Ni_{65}Al_{35}$ alloy, 3R and faulted 14M can replace each other without changing the microtwin plane from wave-like interface and curvature of twin planes. However, according to the above studies, whether the 3R and 14M transformations are independent or 14M is simply a variation of 3R with fine twins accommodating the transformation is still unclear.

Considered the other SMAs, especially 300–500 °C aged Ni-rich TiNi SMAs, multiple-stage martensitic transformations have been intensively studied in which high temperature B2 parent phase transforms to R-phase premartensite and then to B19′ martensite. But under certain aging conditions, there also found that the transformation occurred in three or more stages. These multiple-stage behaviors have been explained by the composition inhomogeneity and/or heterogeneous microstructures which evolves the growth and the size of aged Ti_3Ni_4 precipitates [17–22].

It was shown that the introduction of rhenium into NiAl alloys improved their mechanical properties [23]. Our previous study has showed that, as compared with $Ni_{64}Al_{36}$ SMA, $Ni_{64}Al_{34}Re_2$ SMA can improve the alloy's hot workability and exhibits B2 ↔ $L1_0$(3R) martensitic transformation with M_s temperature at 365.8 K in as-rolled condition [24]. Recently, as-rolled $Ni_{64}Al_{34.5}Re_{1.5}$ SMA was found that it can also improve the alloy's hot workability but it behaves the coexistence of 3R and 14M martensites during the forward martensitic transformation [25]. The aim of the present study is to investigate the 3R and 14M martensitic transformations of as-rolled and 1323 K annealed $Ni_{64}Al_{34.5}Re_{1.5}$ alloy. The characteristics of 3R and 14M transformation exhibited in this alloy will be discussed.

2. Experimental procedures

$Ni_{64}Al_{34.5}Re_{1.5}$ (abbreviated as NiAl–1.5Re) (in at.%) alloy was prepared by the conventional vacuum arc-remelter (VAR) from the raw materials of nickel (purity 99.9 wt.%), aluminum (purity 99.99 wt.%) and rhenium (purity 99.99 wt.%). Alloy with about 100 g weight was melted and remelted at least six times in a low pressure argon atmosphere. Pure titanium bottons were also melted and used as getters. The mass loss during melting was neglected (it was less than 10^{-4}% in weight). Thereafter, the ingot was homogenized at 1473 K for 24 h and cooled in the vacuum furnace, then hot-rolled at 1273 K with ≈1% thickness reduction per pass. After each rolling pass, the rolled-ingot was reheated at 1273 K for at least 6 min, then hot-rolled again for the next pass. The hot-rolling process was stopped when the cracks appeared on the rims of the rolled-ingot. The reduction of thickness was 14.3%. Subsequently, the rolled-ingot was cooled in the air.

The rolled-ingot was cut by a diamond saw to obtain the specimens for the microstructural observation, X-ray diffraction (XRD) measurement, differential scanning calorimetry (DSC) test, microvickers hardness test, etc. Microstructural observations were carried out using optical microscope (OM) and scanning electron microscope (SEM, LEO1530). The etching solution was 45% CH_3COOH, 33% HNO_3, 11% HCl and 11% H_3PO_4 (in volume). The chemical compositions of the observed phases were detected by an electron-probe microanalyzer (EPMA, JOEL JXA-8600SX, standards were $Ni_{50}Al_{50}$, pure Ni, pure Al and pure Re). The composition values were determined from the average of at least 10 measurements for each phase. The specimens for TEM observation (JEOL-100CXII and Philips-TECNAI G^2 20) were prepared by jet polishing in a solution of 10% H_2SO_4 and 90% CH_3OH (in volume) at 263 K. Martensitic transformation temperatures were measured by DSC (TA Q10) equipment with 5 K/min cooling/heating rate. Crystal structures at room temperature were tested by PANalytical X'Pert PRO XRD using Cu Kα radiation and those at higher temperature were carried out in the vacuum with a multipurpose XRD system ("TTRAX III", Rigaku, Japan) using Cu Kα radiation. Microvickers hardness, Hv, was measured by a hardness tester (Mitutoyo HM, Japan) with the applied load and time being 10 g and 15 s, respectively. The Hv values were determined from the average of at least 30 measurements for each specimen.

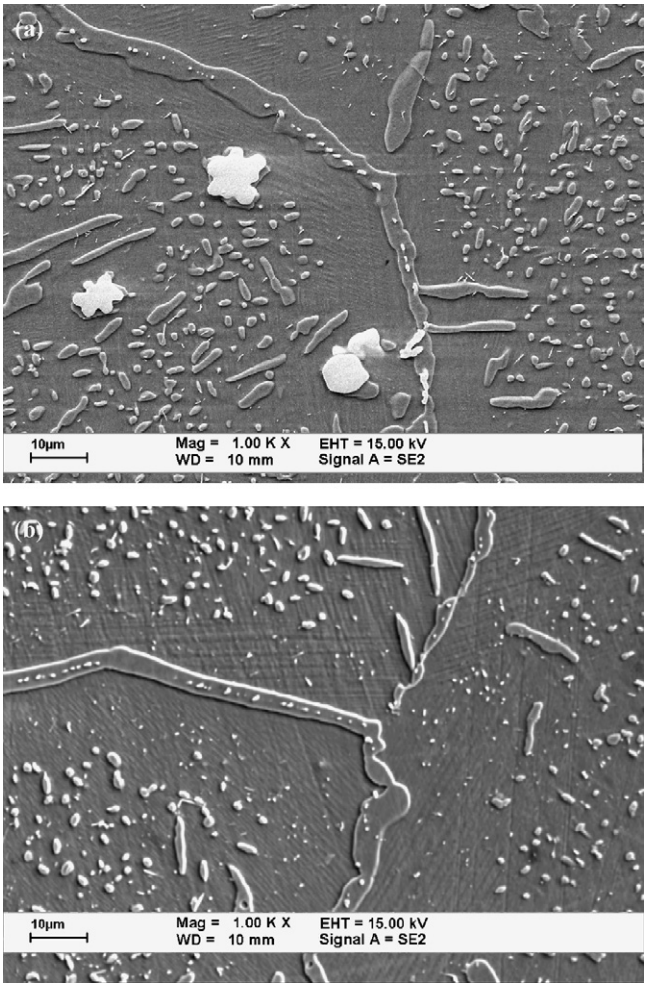

Fig. 1. SEM images of (a) as-rolled NiAl–1.5Re alloy and (b) NiAl–1.5Re alloy annealed at 1323 K for 1 h.

3. Results and discussion

3.1. SEM observation, EPMA detection and hardness test

Fig. 1(a) and (b) shows the SEM images of as-rolled and 1323 K × 1 h annealed NiAl–1.5Re alloy, respectively, which have been etched by the solution. From Fig. 1(a), the stripe/globular shaped Ni_3Al ($L1_2$ structure) and thin continuous plated Ni_3Al ($L1_2$ structure) are precipitated in NiAl matrix (3R & 14M martensites) and along grain boundaries, respectively. There are large white dot-shaped precipitates in the matrix and many tiny white precipitates in the continuous thin Ni_3Al plates along grain boundaries. These are the Re phase soluted with a small amount of Ni [24]. At the same time, from Fig. 1(a), precipitate-free zones (PFZs) along grain boundaries with widths of about 10 μm can be observed. In order to understand the chemical compositions of NiAl and Ni_3Al phases in the matrix and at the grain boundary, as-polished (no chemical-etched) specimens of Fig. 1(a) and (b) are detected by EPMA from one grain to the neighbor grain for at least 60 points and the results are shown in Table 1. From Table 1, the average Ni content in the PFZs of as-rolled specimen is 63.41 ± 0.09 at.%. This is a little lower than the average content in the matrix of about 63.81 ± 0.10 at.%.

Table 1
Compositions of NiAl–1.5Re alloy detected by EPMA from Fig. 1.

Area	Average chemical composition (at.%)[a]			
	Ni	Al	Re	O
As-rolled specimen				
Ni_3Al (at the grain boundary)	75.85 ± 0.09	24.04 ± 0.11	0.06 ± 0.01	0.05 ± 0.01
Ni_3Al (in the matrix)	72.13 ± 0.07	27.75 ± 0.09	0.07 ± 0.01	0.05 ± 0.01
PFZ	63.41 ± 0.09	36.47 ± 0.11	0.05 ± 0.01	0.07 ± 0.01
Matrix	63.81 ± 0.10	36.09 ± 0.12	0.06 ± 0.01	0.04 ± 0.01
1323 K × 1 h annealed specimen				
Ni_3Al (at the grain boundary)	75.13 ± 0.07	24.76 ± 0.09	0.07 ± 0.01	0.04 ± 0.01
Ni_3Al (in the matrix)	72.60 ± 0.08	27.29 ± 0.10	0.05 ± 0.01	0.06 ± 0.01
PFZ	64.32 ± 0.07	35.57 ± 0.09	0.06 ± 0.01	0.05 ± 0.01
Matrix	64.43 ± 0.09	35.47 ± 0.11	0.05 ± 0.01	0.05 ± 0.01

[a] The chemical composition of each area is measured at least 10 points.

After NiAl–1.5Re alloy is annealed at 1323 K for 1 h, as shown in Fig. 1(b), Ni_3Al precipitates in the matrix are fewer and smaller than those in Fig. 1(a). At that time, the Ni content in the PFZs and in the matrix increases to 64.32 ± 0.07 at.% and 64.43 ± 0.09 at.%, respectively, as shown in Table 1.

Fig. 2 shows the Hv hardness results of NiAl–1.5Re alloy. From Fig. 2, the average Hv values of as-rolled NiAl–1.5Re in the matrix and in the PFZs are 221.6 ± 8.6 and 244.8 ± 9.2, respectively. Obviously the hardness in the PFZs is higher than that in the matrix. Also from Fig. 2, after annealing at 1323 K for 1 h, the hardness of NiAl–1.5Re alloy decreases to 200.8 ± 6.5 in the PFZs and 198.7 ± 9.3 in the matrix with no significant difference in between the two values. It is worthy to note that, for both as-rolled and annealed specimens, although the Ni content in the PFZs is a little lower than that in the matrix, the hardness difference between the PFZs and the matrix is significant in as-rolled specimen but is almost the same in annealed specimen. This characteristic will be discussed in Section 3.5.

3.2. DSC measurement

Fig. 3(a) shows the DSC curve of as-rolled NiAl–1.5Re alloy which exhibits a two-step transformation upon cooling. In order to understand the characteristics of the two transformation peaks shown in Fig. 3(a), partial-cycle DSC test is performed. As seen in Fig. 3(a), when the specimen is cooled to approach peak 1 (332.6 K) and then instantly heated up, a new peak, peak 3, appears at 356 K which is not obviously in the full-cycle DSC curve. The hysteresis of peaks 1 and 3 is 23.4 K. Also seen in Fig. 3(a), when the specimen is cooled to peak 2 (314.8 K) and then instantly heated up, peak 4 appears at 349 K which is almost consistent with the peak found in the full-cycle DSC curve. The hysteresis of peaks 2 and 4 is about 34.2 K. Most probably, peaks 1 and 3 and peaks 2 and 4 correspond to individual martensitic transformation, as further discussed in Section 3.5.

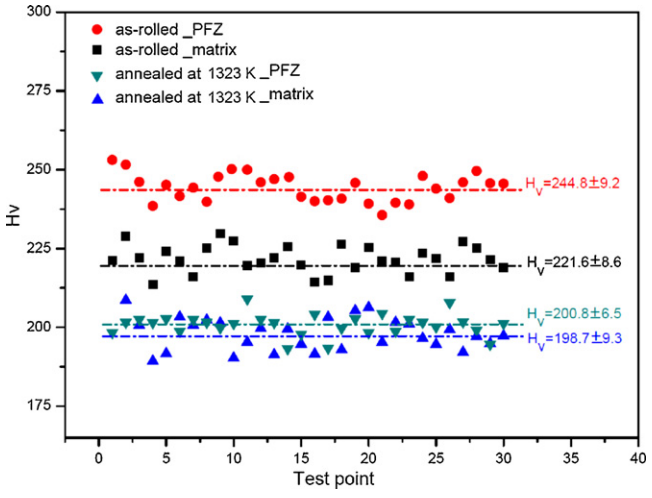

Fig. 2. The microvickers Hv hardnesses of the precipitate-free zone (PFZ) and the matrix in as-rolled NiAl–1.5Re alloy and NiAl–1.5Re alloy annealed at 1323 K for 1 h.

In order to understand the effect of the annealing temperature on martensitic transformation, NiAl–1.5Re alloy annealed at 1323 K for 1 h is also tested by DSC and the full-cycle and partial-cycle DSC results are shown in Fig. 3(b). From Fig. 3(b), only one exothermic peak, instead of two peaks, can be observed in the cooling curve and its M_s temperature and ΔH value increase significantly to 382.5 K and 5.1 J/g, respectively. Also from Fig. 3(b), the hysteresis of transformation peaks for forward and reverse transformation is 30.5 K, which is larger than that of peaks 1 and 3 but lower than that of peaks 2 and 4, as shown in Fig. 3(a).

3.3. XRD test

Fig. 4(a) and (b) shows the XRD profiles obtained at room temperature for as-rolled and 1323 K × 1 h annealed NiAl–1.5Re alloy, respectively. From Fig. 4(b), the significant diffraction peaks of 1323 K annealed specimen are identified as B2 parent phase, Ni_3Al phase, Re phase and 3R martensite, which are similar to those of 1373 K × 1 h annealed NiAl–2.0Re alloy [24]. From Fig. 4(a), except those significant diffraction peaks shown in Fig. 4(b), there is one additional and obvious diffraction peak located at $2\theta = 46.18^\circ$ and it appears in between $(1\,1\,0)_{B2}$ and $(2\,0\,0)_{3R}$ peaks. In accordance with Ref. [16], this additional peak is identified as $(1\bar{1}7)_{14M}$ peak of 14M martensite. Notice that there is no $(1\bar{1}7)_{14M}$ peak in Fig. 4(b). Obviously, 3R and 14M martensites coexist at room temperature in as-rolled NiAl–1.5Re alloy. In order to further understand the 3R and 14M martensitic transformations exhibited in as-rolled NiAl–1.5Re alloy, high temperature XRD test with a complete scan ($2\theta = 20$–90°) is performed over the temperature range from 373 K to 173 K and the results are shown in Fig. 5. In Fig. 5, the specimen is first heated up to 373 K in which the XRD pattern shows B2 phase, Ni_3Al phase, Re phase and retained 3R martensite. Thereafter, the specimen is cooled from 373 K with the cooling rate of 2 K/min. The $(1\bar{1}7)_{14M}$ peak first appears at 333 K which is close to M_s temperature of the higher temperature peak (≈338.6 K) shown in DSC cooling curve of Fig. 3(a). As the testing temperature further decreases, the intensity of $(1\bar{1}7)_{14M}$ peak increases continuously. At the same time, the intensity of $(2\,0\,0)_{Ni3Al}$ peak remains almost the same. This means that the intensity increase of the diffraction peak $\{(1\,1\,1)_{3R} + (1\,1\,1)_{Ni3Al}\}$ located at $2\theta = 43.76^\circ$, as indicated by the arrow, is due to the intensity increase of $(1\,1\,1)_{3R}$ peak. Also from Fig. 5, the intensity of $(1\,1\,0)_{B2}$ peak decreases continuously as the temperature decreases. Obviously, the B2 phase transforms to 14M and 3R martensites simultaneously during the cooling from 333 K to 173 K.

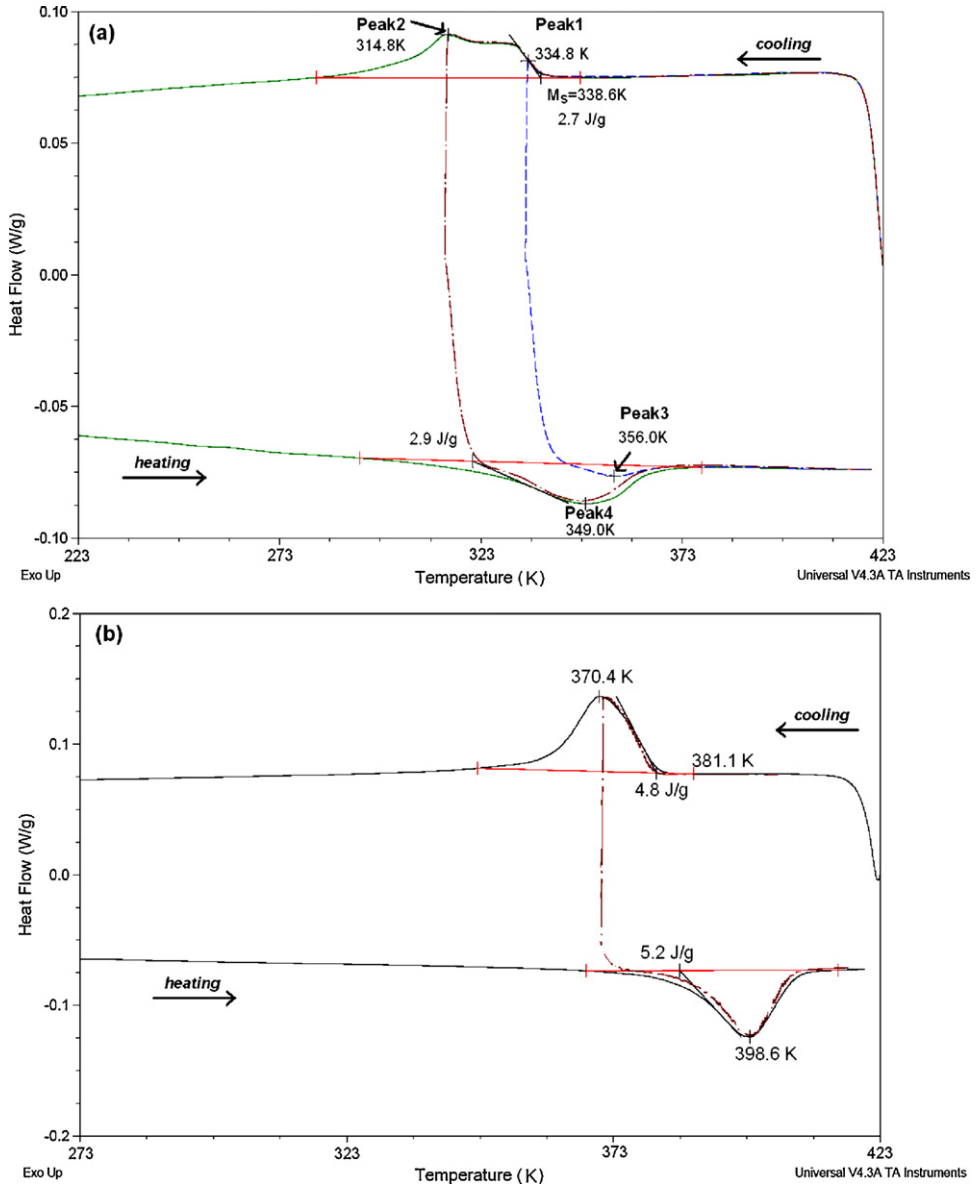

Fig. 3. DSC curves of (a) as-rolled NiAl–1.5Re alloy and (b) NiAl–1.5Re alloy annealed at 1323 K for 1 h. Partial cycling DSC tests are also shown in (a) and (b).

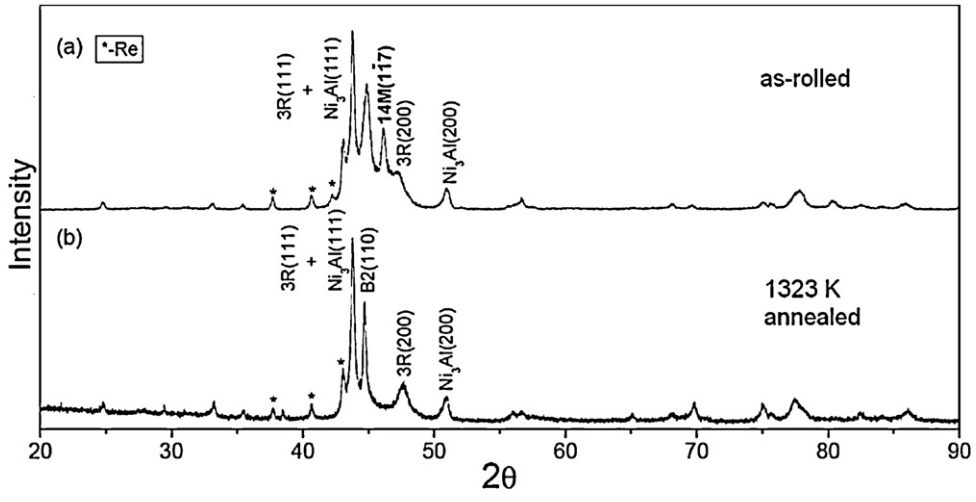

Fig. 4. XRD patterns tested at room temperature for (a) as-rolled NiAl–1.5Re alloy and (b) NiAl–1.5Re alloy annealed at 1323 K for 1 h.

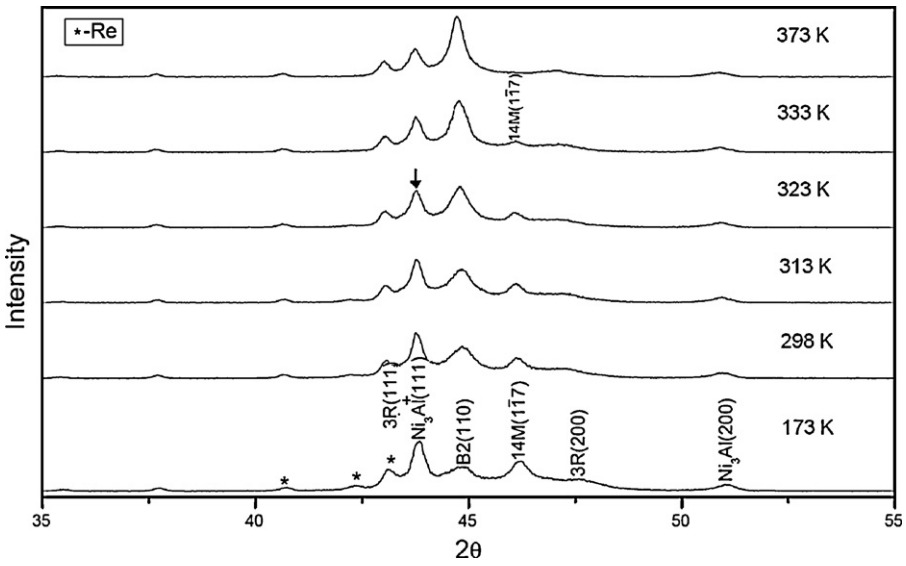

Fig. 5. High-temperature XRD scans of the as-rolled NiAl–1.5Re alloy, starting at 373 K (top) and continuing down to 173 K (bottom) with a cooling rate of 2 K/min.

3.4. TEM observation

The TEM bright-field (BF) images and the selected area diffraction pattern (SADP) of as-rolled NiAl–1.5Re specimen taken at room temperature are shown in Fig. 6. Fig. 6(a) is the BF image and Fig. 6(b) is the enlarged micrograph of the square area shown in Fig. 6(a). From Fig. 6(a) and (b), rod-like/globular shape Ni_3Al particles are precipitated in the NiAl matrix and there are many Re phase precipitated in Ni_3Al particles and in the matrix, as indicated by the arrows. The NiAl matrix shown in Fig. 6(b) has two kinds of

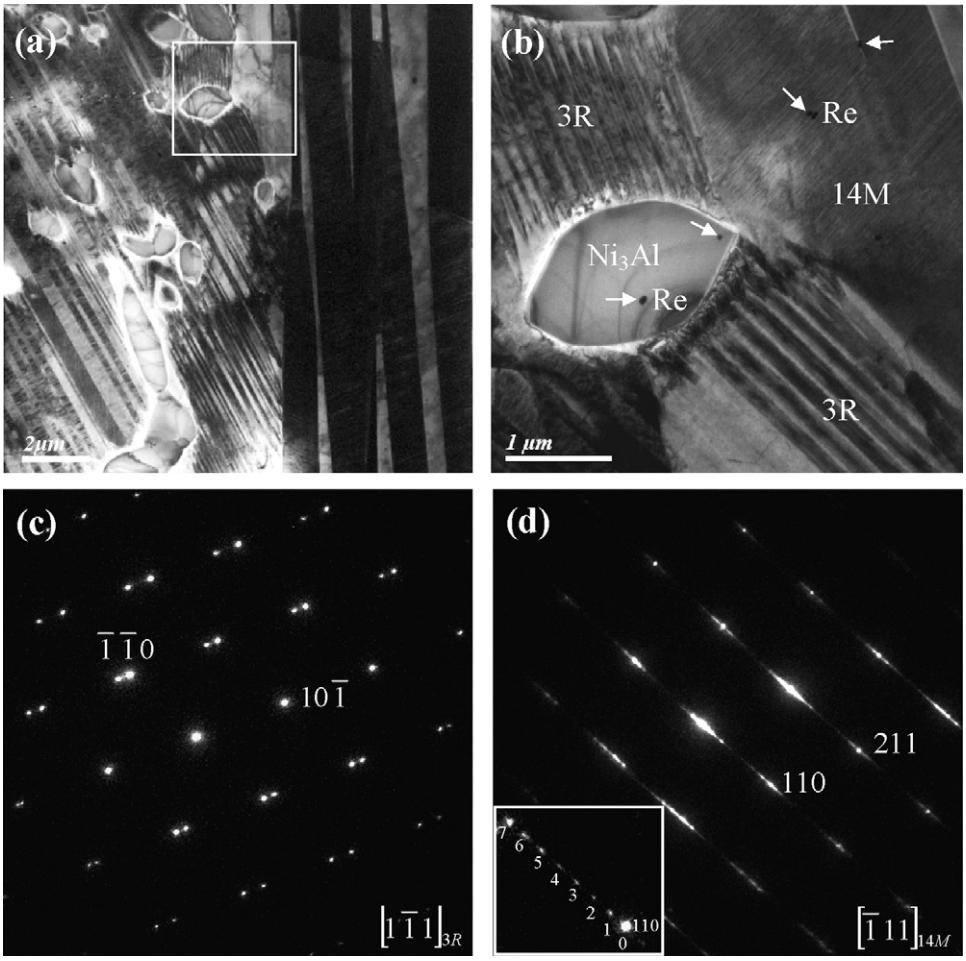

Fig. 6. (a) BF image of as-rolled NiAl–1.5Re alloy in which a rod-like/globular shape Ni_3Al in NiAl martensite. (b) The magnification of the square area shown in (a). (c) SADP of 3R martensite with $[1\bar{1}1]_{3R}$ zone axis and (d) SADP of 14M martensite with $[\bar{1}11]_{14M}$ zone axis.

microstructural morphologies, which are indicated as 3R and 14M. Fig. 6(c) and (d) are the SADPs of these two different morphologies and they are identified as 3R and 14M martensites, respectively. Here, 14M martensite shows fine twins and has a row of seven super-reflections, as shown in the inset of Fig. 6(d) [26]. The result of Fig. 6 also supports the XRD evidence of Fig. 4(a) for the coexistence of 3R and 14M martensites in as-rolled NiAl–1.5Re alloy at room temperature. From Fig. 6(a), one can find that the 3R martensite forms in the matrix which has a lot of Ni_3Al precipitates but the 14M martensite forms in the PFZs without Ni_3Al precipitates.

3.5. Discussion of the characteristics of 3R and 14M martensitic transformations

Jee et al. [27] reported that there are small XRD peaks with a low resolution in between $(1\,1\,1)_{3R}$ and $(2\,0\,0)_{3R}$ peaks in $Ni_{63.8}Al_{36.2}$ alloy prepared by PM method. They proposed that this feature might be related to the appearance of a small amount of 14M martensite. In their study, they found two peaks in DSC cooling curve in which the peak height of the higher temperature peak was higher than that of the lower one. However, there was no further discussion to confirm which transformation peak corresponded to B2 → 3R (or B2 → 14M). According to the present study, two apparent transformation peaks shown in DSC cooling curve of as-rolled NiAl–1.5Re alloy have confirmed to correspond to two transformations of B2 → 14M and B2 → 3R. However, which peak corresponding to B2 → 14M (or B2 → 3R) is still unknown. In Fig. 5, 14M martensite starts to appear as the temperature decreases to 333 K which is close to the M_s = 338.6 K for the higher temperature peak of DSC cooling curve shown in Fig. 3(a). This implies that the higher temperature peak in the DSC cooling curve corresponds to B2 → 14M transformation. Meanwhile, in Fig. 3(a), the hysteresis of peak 1 and peak 3 is 21.2 K which is much smaller than that of peak 2 and peak 4, around 34.2 K. Since 14M martensite has a high density of twinning planes, as shown in Fig. 6(b), the elastic energy can be stored in twinning planes during the forward transformation and is released during the reverse transformation. This feature may cause B2 ↔ 14M to have lower transformation hysteresis than B2 ↔ 3R. From the above discussion, the higher and lower temperature peaks appearing in DSC cooling curve of Fig. 3(a) can be identified as B2 → 14M and B2 → 3R transformation, respectively. Moreover, from Fig. 5, the B2 phase transforms to 3R and 14M martensites simultaneously, even if the temperature decreases to 173 K. This implies that the 14M martensite may be not a premartensite of B2 → 3R transformation, and B2 ↔ 3R and B2 ↔ 14M are two independent martensitic transformations. These characteristics can also be confirmed from the reverse transformation peaks shown in Fig. 3(a) in which 3R → B2 and 14M → B2 transformations are independent.

After annealing at 1323 K × 1 h, NiAl–1.5Re alloy has only 3R martensite at room temperature and the hardnesses in the PFZs and in the matrix are almost the same. This feature is similar to that in NiAl–2.0Re alloy annealed at 1373 K × 1 h in which only 3R martensite is observed at room temperature [24,25]. We propose that the hardnesses of NiAl–1.5Re specimen in the PFZs and in the matrix depend on both the Ni content and the martensite structure. From Table 1 and Fig. 2, the higher the Ni content in the martensite is, the lower the hardness it has. At the same time, the 14M martensite is harder than the 3R martensite. This comes from the fact that the 14M martensite has a high density of periodic stacking faults [5]. From Fig. 6(a), the 14M martensite forms in the PFZs without Ni_3Al particles. Cui et al. [28] reported that the formation of PFZs in NiAl SMAs results from the consumption of Ni atoms in the formation of Ni_3Al. This feature can explain why the Ni content in the PFZs is lower than that in the matrix, as indicated in Table 1. Yang and Wayman suggested that Ni–Al binary SMAs with Ni content greater than 63.0 at.% transform to 3R martensite, and those with Ni content less than 63.0 at.% transform to 14M martensite [9]. From the composition of PFZs shown in Table 1, it is speculated that the critical composition of 63.0 at.% Ni for Ni–Al binary alloy may shift to around 63.6 at.% for NiAl–1.5Re alloy because some Al atoms in $Ni_{64}Al_{36}$ alloy are replaced by Re atoms. Kainuma et al. [29] found that, in addition to 3R martensite, 14M martensite was present while adding Ti, Mo, Ag, Ta or Zr to the binary $Ni_{64}Al_{36}$ alloy. They proposed that the appearance of the 14M martensite was attributed to the solid solution hardening arising from the difference in atomic sizes among Ni, Al and the third element added. We suggest that, in addition the solid solution hardening by adding Re, Ni-depletion in the PFZs is the another reason that leads to the appearance of 14M martensite, as shown in Fig. 6 and Table 1. After NiAl–1.5Re alloy is annealed at 1323 K × 1 h, only 3R and no 14M can be observed. The Ni content of annealed alloy is higher than 63.6 at.% both in the PFZs and in the matrix.

4. Conclusions

Specimens of as-rolled and 1323 K × 1 h annealed NiAl–1.5Re SMA were examined by SEM/TEM, DSC, XRD, EPMA and hardness Hv tests. Experimental results show that both B2 ↔ 14M and B2 ↔ 3R martensitic transformations are exhibited in as-rolled alloy, but only B2 ↔ 3R appears in annealed alloy. For as-rolled specimen, two peaks appear in DSC cooling curve. According to the XRD results tested from 373 K to 173 K and the transformation hysteresis measured by partial-cycle DSC tests, the higher temperature peak with M_s = 338.6 K is identified as B2 → 14M transformation and the lower temperature peak as B2 → 3R. Hardness tests show that the hardness of 14M martensite is higher than that of 3R because the 14M martensite has many intrinsic periodic stacking faults. TEM observations and EPMA measurements indicate that, for as-rolled NiAl–1.5Re alloy, the 14M martensite is formed in the PFZ which is a Ni-depletion region and 3R martensite is formed in the matrix which is a Ni-enrichment region. The critical Ni content for the 14M martensite can be formed is lower than about 63.6 at.% for NiAl–1.5Re alloy, as compared to 63.0 at.% for Ni–Al binary alloy. The shift of the critical value may come from the effect of the solid solution hardening by adding Re in NiAl–1.5Re alloy. If this alloy is annealed at 1323 K × 1 h, only B2 ↔ 3R transformation can be observed because the Ni content of this alloy is higher than 63.6 at.% both in the PFZs and in the matrix.

Acknowledgement

The authors gratefully acknowledge the financial support of this study from the National Science Council (NSC), Taiwan, Republic of China, under the Grant NSC97-2221-E002-035-MY3.

References

[1] James L. Smialek, Robert F. Hehemann, Metall. Trans. 4 (1973) 1571–1575.
[2] K. Enami, S. Nenno, Metall. Trans. 2 (1971) 1487–1490.
[3] K. Otsuka, T. Ohba, M. Tokonami, C.M. Wayman, Scripta Metall. Mater. 29 (1993) 1359–1365.
[4] F. Reynaud, Scripta Metall. 11 (1977) 765–770.
[5] V.V. Martynov, K. Enami, L.G. Khandros, A.V. Tkachenko, S. Nenno, Scripta Metall. 17 (1983) 1167–1171.
[6] Y.K. Au, C.M. Wayman, Scripta Metall. 6 (1972) 1209–1214.
[7] Y. Murakami, K. Ohtsuka, S. Hanada, S. Watanabe, Mater. Trans. JIM 17 (1992) 282–288.
[8] D. Schryvers, L.E. Tanner, Ultramicroscopy 32 (1990) 241–254.
[9] J.H. Yang, C.M. Wayman, Intermetallics 2 (1994) 111–119.
[10] T. Inoue, S. Morito, Y. Murakami, K. Oda, K. Otsuka, Mater. Lett. 19 (1994) 33–37.
[11] A.G. Khachaturyan, S.M. Shapiro, S. Semenovskaya, Phys. Rev. B 43 (1991) 10832–10843.
[12] P.S. Khadkikar, I.E. Locci, K. Vedula, G.M. Michal, Metall. Trans. A 24 (1993) 83–94.
[13] A.S. Murthy, E. Goo, Acta Mater. 41 (1993) 3435–3443.

[14] E.P. George, C.T. Liu, J.A. Horton, C.J. Sparks, M. Kao, H. Kunsman, T. King, Mater. Charact. 32 (1994) 139–160.
[15] P.L. Potapov, S.Y. Song, V.A. Udovenko, S.D. Prokoshkin, Metall. Trans. A 28 (1997) 1133–1142.
[16] P.L. Potapov, P. Ochin, J. Pons, D. Schryvers, Acta Mater. 48 (2000) 3833–3845.
[17] J.K. Allafi, X. Ren, G. Eggeler, Acta Mater. 50 (2002) 793–803.
[18] M. Nishida, T. Hara, T. Ohba, K. Yamaguchi, K. Tanaka, K. Yamauchi, Mater. Trans. 44 (2003) 2631–2636.
[19] A. Dlouhy, J.K. Allafi, G. Eggeler, Philos. Mag. 83 (2003) 339–363.
[20] J.K. Allafi, G. Eggeler, A. Dlouhy, W.W. Schmahl, Ch. Somsen, Mater. Sci. Eng. A 378 (2004) 148–151.
[21] J. Michutta, Ch. Somsen, A. Yawny, A. Dlouhy, G. Eggeler, Acta Mater. 54 (2006) 3525–3542.
[22] G. Fan, Y. Zhou, W. Chen, S. Yang, X. Ren, K. Otsuka, Mater. Sci. Eng. A 438–440 (2006) 622–626.
[23] V.E. Oliker, E.N. Eliseeva, T.Ya. Gridasova, I.I. Timofeeva, A.V. Kotko, Powder Metall. Met. Ceram. 49 (2010) 245–252.
[24] H.J. Kang, S.K. Wu, L.M. Wu, Intermetallics 18 (2010) 123–128.
[25] H.J. Kang, S.K. Wu, unpublished work, 2009.
[26] K. Enami, A. Nagasawa, S. Nenno, Scripta Metall. 12 (1978) 223–226.
[27] K.K. Jee, P.L. Potapov, S.Y. Song, M.C. Shin, Scripta Metall. 36 (1997) 207–212.
[28] Y.X. Cui, L. Zhen, D.Z. Yang, G.P. Bi, Q. Wang, Mater. Lett. 48 (2001) 121–126.
[29] R. Kainuma, H. Ohtani, K. Ishida, Metall. Trans. A 27 (1996) 2445–2453.